Universiteit Antwerpen

This item is the archived peer-reviewed author-version of:

Automated thermographic detection of blood vessels for DIEP flap reconstructive surgery

Reference:
Cardenas Edgar, Verstockt Jan, Verspeek Simon, Clarys Warre, Thiessen Filip, Tondu Thierry, Tjalma Wiebren, Steenackers Gunther, Vanlanduit Steve.-
Automated thermographic detection of blood vessels for DIEP flap reconstructive surgery
International journal of computer assisted radiology and surgery - ISSN 1861-6410 - 19:9(2024), p. 1733-1741
Full text (Publisher's DOI): https://doi.org/10.1007/S11548-024-03199-8
To cite this reference: https://hdl.handle.net/10067/2068800151162165141

uantwerpen.be
Institutional repository IRUA

Automated thermographic detection of blood vessels for DIEP flap reconstructive surgery

Edgar Cardenas De La Hoz[1*†], Jan Verstockt[1†], Filip E.F. Thiessen[2,3], Thierry Tondu[2,3], Simon Verspeek[1], Wiebren A.A. Tjalma[4], Gunther Steenackers[1], Steve Vanlanduit[1]

[1*]InViLab Research Group, Faculty of Applied Engineering, University of Antwerp, Groenenborgerlaan 171, Wilrijk, 2020, Antwerp, Belgium.
[2]Department of Plastic, Reconstructive and Aesthetic Surgery, Multidisciplinary Breast Clinic, Antwerp University Hospital, Wilrijkstraat 10, Antwerp, 2650, Antwerp, Belgium.
[3]Department of Plastic, Reconstructive and Aesthetic Surgery, Ziekenhuis Netwerk Antwerpen, Lindendreef 1, Antwerp, 2020, Antwerp, Belgium.
[4]Gynaecological Oncology Unit, Department of Obstetrics and Gynaecology, Multidisciplinary Breast Clinic, Antwerp University Hospital, Wilrijkstraat 10, Antwerp, 2650, Antwerp, Belgium.

*Corresponding author(s). E-mail(s): edgar.cardenas@uantwerpen.be;
Contributing authors: jan.verstockt@uantwerpen.be;
†These authors contributed equally to this work.

Abstract

Purpose: Inadequate perfusion is the most common cause of partial flap loss in tissue transfer for post mastectomy breast reconstruction. The current state-of-the-art uses Computed Tomography Angiography (CTA) to locate the best perforators. Unfortunately, these techniques are expensive and time-consuming and not performed during surgery. Dynamic infrared thermography (DIRT) can offer a solution for the disadvantages.

Methods: The research presented couples thermographic examination during DIEP flap breast reconstruction with automatic segmentation approach using a convolutional neural network. Traditional segmentation techniques and annotations by surgeons are used to create automatic labels for the training.

Results: The network used for image annotation is able to label in real-time on minimal hardware and the labels created can be used to locate and quantify perforator candidates for selection.
Conclusions: These results allow for a computational system that can be used in place during surgery to improve surgical success.

Keywords: thermography, DIEP flap, artificial intelligence, machine learning, dynamic infrared thermography, reconstructive surgery, convolutional neural networks, perforator blood vessel, breast reconstruction

1 Introduction

Breast cancer is a significant health concern globally, affecting millions of people each year. Breast cancer is the most diagnosed cancer in women worldwide, accounting for nearly 25% (24.5%) of all cancer cases [1]. Belgium exhibits the highest per capita incidence of breast cancer in women, with a rate of 113.2 cases per 100,000 individuals, resulting in more than 11,000 new cases annually, as reported by the World Health Organization. [1, 2]. However, improvements in screening methods, advancements in treatment options, and increased awareness have also contributed to higher survival rates [1, 3]. Among breast cancer patients, approximately one-third (34%) undergo either unilateral or bilateral mastectomy, with 1 out of 7 patients opting for reconstructive surgery. Among these reconstructive procedures, half involve the use of autologous tissue. Specifically, 32% of the autologous tissue flaps employed in reconstructive surgeries are Deep Inferior Artery Epigastric Perforator (DIEP) flaps [1, 2, 4]. Autologous tissue refers to biological tissue harvested from an individual's own body and used for medical purposes, providing compatibility and minimizing the risk of rejection compared to tissues sourced from others or different species. The significant number of new cases underscores the importance of ongoing research and effective healthcare strategies to address this prevalent health concern.

1.1 DIEP flap procedure

Deep Inferior Epigastric artery Perforator flap (DIEP flap) has become the standard procedure for autologous breast reconstruction after mastectomy. During this procedure, the fat and skin from the abdomen are transplanted to the chest. A major challenge encountered from the procedure is the selection of a suitable perforator to provide sufficient blood supply for the transplanted tissue, including the determination of the perfused area of the chosen perforator [5]. The main method used for perforator mapping is Computed Tomography Angiography (CTA). Figure 1 shows an abdomen annotated by the surgeon using the mapping of the CTA. However, this is a relatively expensive imaging method that requires intravenous contrast injection, exposes patients to ionizing radiation and must be done prior to the surgery and does not give any information on the tissue perfusion [6]. Further comparison is shown in table 1.

	CTA	DIRT
Imaging Location	- Hospital	- Private clinic - Doctor's office - Hospital
Timing	- Prior to surgery	- Prior to surgery - During Surgery - After Surgery
Pro	- High resolution - 3D imaging - Perforator coordinates - Perforator route	- Fast - Portable - Inexpensive - Detection of perfused area - Anastomosis check during surgery - Non-contact
Con	- Harmful radiation - Contrast fluid injection - Expensive - Only prior to surgery - No information on perfused area - No information on blood supply	- Thermal excitation (cooling) - Low resolution - No exact perforator coordinates - No perforator routing information - 2D thermal information

Table 1 Comparison between Computer Tomography Angiography (CTA) and Dynamic Infrared Thermography (DIRT) based on [2]

1.2 Dynamic Infrared Thermography

Infrared Thermography (IR) has been demonstrated for numerous biomedical applications including the detection of cancer and vascular disorders by allowing precise measurements of temperature differences in the body. Previous work has even been performed for the automatic detection of perforators using IR thermography for the DIEP flap procedure [7]. Unfortunately, in much of this work, static measurements are taken which severely limits the thermal properties that are quantified using active modalities. Active infrared thermography can provide higher sensitivity to temperature variations, allowing for the detection of smaller defects or anomalies [8]. Dynamic measurements are achieved by first cooling the target tissue and using thermography to measure the change and reveal important information about physiological properties such as blood flow and perfusion area that cannot be seen in static reading. Dynamic Infrared Thermography (DIRT) has been proposed as an alternative imaging modality for perforator identification and localization to replace CTA because of the ability of the technique to detect vascular structures and their features deeper in the body. [9, 10]. Perforators responsible for blood transportation to the subdermal plexus induce localized thermal elevation on the skin surface [10]. This methodology finds applicability across the preoperative, perioperative, and postoperative phases.

1.3 Automated Preforator Detection

Prior work has been done to automate the perforator selection, specifically for DIEP flap surgery, often emphasizing the importance of reducing labour and time for interpreting the results. In Mavioso et al, a method for perforator detection using CTA is developed using traditional segmentation techniques. In CTA, this is especially useful as a radiologist is often needed for the interpretation of angiograms. Removing the need for specialists can increase accessibility and turnover time for the procedure [11].

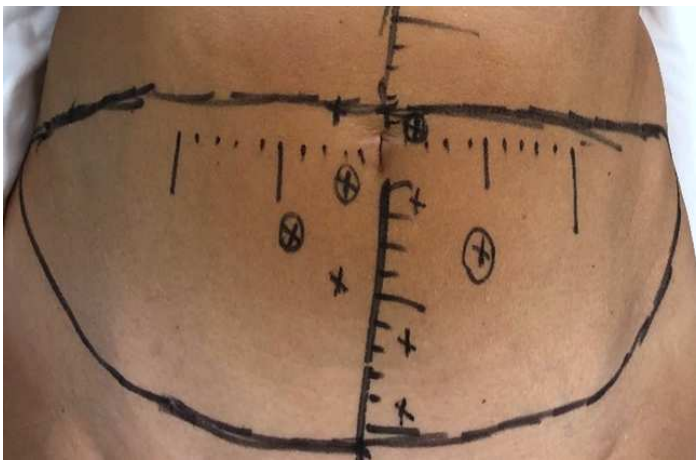


Fig. 1 RGB Image of abdominal section with annotations of CTA results by surgeon

Similarly, Kakileti et al, aim to automate breast cancer screening using thermography. In this work, detection and quantification of blood vessel morphology are achieved using background subtraction, vesselness filters and threshold segmentation. In this application, the importance of standardized quantification is essential, as a subjective interpretation of the thermographic readings is a barrier to adopting the technology [12]. Lastly, both works involve the use of traditional segmentation techniques that are highly sensitive to noise and lighting changes that a human could easily ignore. Mavioso [11] concludes that their proposed method could be improved using machine learning and neural network-based methods that have become prevalent in order to become more robust.

Also noted is the requirement of neural network-based methods on specialized hardware or server connection that make them impractical to use in medical applications or real-time settings. For any proposed method in this domain to be useful, it will be necessary for the network to be executable on local reasonably powerful hardware.

2 Methodology

The proposed pipeline as shown in figure 2 details the detection methodology from image capturing to measurement of detected regions.

2.1 Imaging Procedure

The dynamic thermography protocol from Thiessen et al.[13] was used for imaging. In this work, it was determined that cooling the desired area with an ice-water bag was the best method for imaging in the constraints of a surgical setting. Skin rewarming was monitored for at least 5 minutes after cooling. As seen in figure 3, camera measurements were taken using a Xenics Gobi+640 (Xenics, Belgium), positioned between 1.0-1.2 meters above the patient while the patient is lying flat. The distance of the

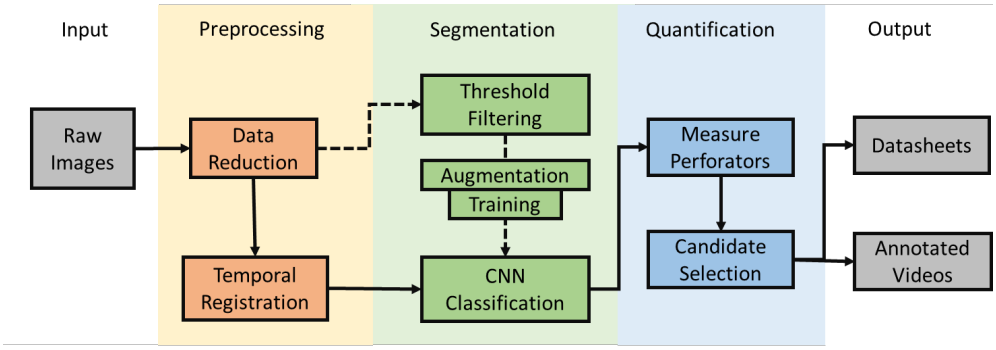


Fig. 2 RGB Image of abdominal section with annotations of CTA results by surgeon

camera varies depending on the height of the surgery table (preference of the surgeon), size of the patient and obstructing medical devices above the surgery table. Some images were taken during the pre-surgery examination while others were at the start of the surgery. Ground truth for the perforator locations was determined using CTA by the surgeon and the radiology staff as the standard procedure. The Xenics Gobi+640 is an uncooled, long-wavelength (8-14μm) microbolometer camera and is chosen because of its compact size, high image resolution (640 x 480 pixels), and low detector NETD (Noise Equivalent Temperature Difference $<$ 30 mK at 300 Kelvin)[13]. Detailed hardware requirements can be found in table 2.



Fig. 3 Thermal Camera, unobtrusively set up in the operating room above patient and surgical staff

Camera	Hardware	Software
Xenics Gobi NETD: <30mK@300K Framerate: 30 Hz Spectral range: 8 - 14 μm	Intel Core i7 Nvidia GPU	Python 3.8 > Pytorch 1.7.0 > CUDA 11

Table 2 Data acquisition and processing setup

2.2 Compression and Storage

Images from the Xenics Gobi+640 are natively in uint16 at 30 Hz. It is necessary to compress the raw data from the cameras taken at 30 Hz to 1 Hz, a frame rate that can be processed by a neural network. In addition to sub-sampling, the image data in uint16 format is converted to uint8 format. Conversion is performed as follows: Intensity values are clipped from the camera at values 0°C to 40°C and normalizing to uint8 dynamic range.

2.3 Registration and Stabilization

While the camera assembly is securely mounted, patient respiration causes periodic movement over a time-lapse measurement. This can cause artifacts while attempting to quantify temporal changes using point wise measurements. Therefore it is necessary to utilize temporal registration techniques to remove movement and stabilize the image data over time. For that reason, stabilization was performed by using the phase correlation technique [14]. This method uses a cross-correlation of the phase component of the images' FFT transforms to return rigid deformations. This approach can calculate the transformations between sequential images and transform them to produce stabilized timelapse images. An example of a stabilized image can be seen in figure 4. An additional benefit of the FFT approach is that the cross-correlation coefficient between images can be used to identify large changes between images when the sum of the amplitude of the cross-correlation is low. The latter is useful for automatically determining the first time point of the cooling challenge as when the cooling bag is removed and no longer obstructing the abdominal region or when there is a significant obstruction in the image, such as the surgeon's hands, that would indicate that the image should be ignored during measurement.

2.4 Segmentation and Classification

Once an image set with the cooling challenge has been processed, labels are generated using standard threshold-based image segmentation on two images taken during the challenge. The first image is captured immediately after cooling and the second is captured after reheating as occurred. Four label classes are created for preoperative image data. An example of these images and labels are shown in figure 5. An overview of the classes and their characteristics can be found in table 3.

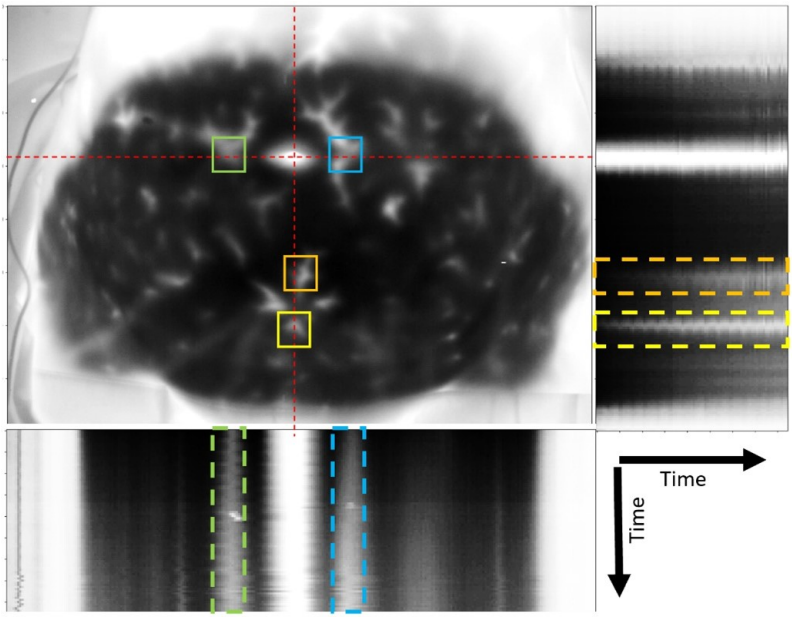


Fig. 4 Top Left: Thermographic Image of abdominal reheating. Top Right: Kymograph of Y slice. Bottom Left: Kymograph of X slice.

Class 1: Cooled Abdomen
This is segmented with thresholding low values on the first time-lapse frame after cooling has begun. It is within this region that all other class labels must exist.
Class 2: Umbilicus
The umbilicus is a high-temperature region that exists in the top center of the cooled abdomen region. This region does not significantly change in intensity over time. Detecting the umbilicus is essential to detect because it acts as a position reference for localization and comparing with CTA.
Class 3: Perforators
These can be found by selecting the regions within the abdomen that contain intensity values above a given threshold in the endpoint image and cooled in the starting image. Perforators are often long and star-shaped and must be above a given size to be considered. Perforators candidates that are close to the umbilicus on either side are considered to be the best for transplants.
Class 4: Cooling Artifacts
This class is for uneven cooling lines from the bag on the skin. These are lines that are more intense than the abdomen in the early images but slowly converge over time to the rest of the abdomen. These regions can appear similar to perforators given their geometry and therefore adding them as a separate class trained with a negative loss is used in training a network not to detect false positives.

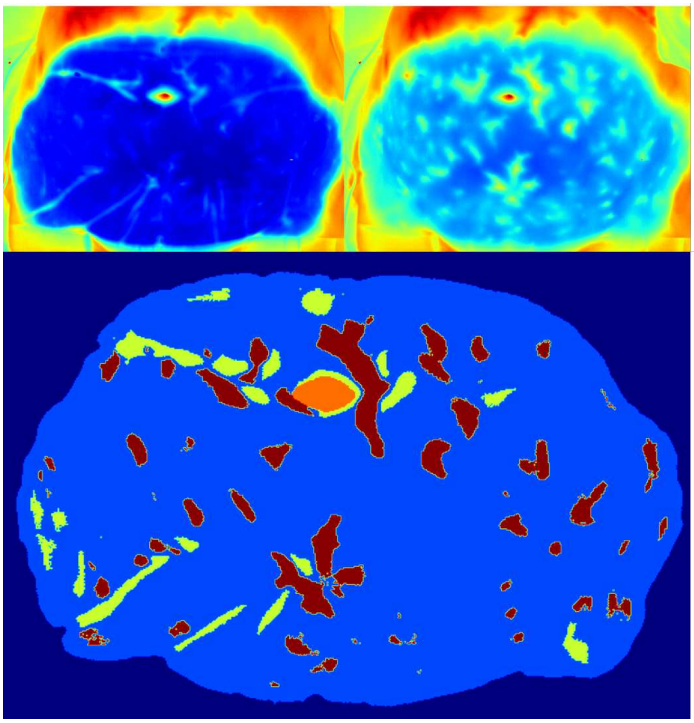


Fig. 5 Left (Immediately after cooling), Right (After 5 minutes of reheating) Bottom: Segmentation of Abdominal section: Unclassed(Dark Blue), Abdomen(Light Blue), Umbilius(Orange), Perforators(Red), Cooling artifacts(Green)

	Class	**Color**	T_0	T_x
1	Cooled Abdomen	Light blue	Low	Medium
2	Umbilicus	Orange	High	High
3	Perforators	Red	Low	High
4	Cooling artifacts	Green	Medium	Medium
	Unclassed	Dark Blue		

Table 3 Overview of segmentation classes and qualities

2.5 Perforator Measurement

Once candidate regions have been detected by the segmentation algorithm, individual perforator detections must be quantified to determine which candidate is the best for use in transplantation. The criteria for best usage are strong reheating and separation from other perforators, which are proxy indicators for higher blood flow and having a large feeding area.

2.6 Machine Learning

While effective in controlled conditions, the use of intensity and area thresholds to segment different regions is not robust enough to be practical for all uses. These specific

techniques can easily error when presented with changes in illumination, noise and camera angles. To create a more robust detection system, a dataset of thermographic scans was subjected to augmentation methods and corrosive warping transformations and used to train a convolutional neural network. Ground truth was determined by curating the results from the threshold segmentation. These results were further verified by input from the surgeon as to which perforators were the best candidates according to the CTA measurements.

2.7 Network Architecture

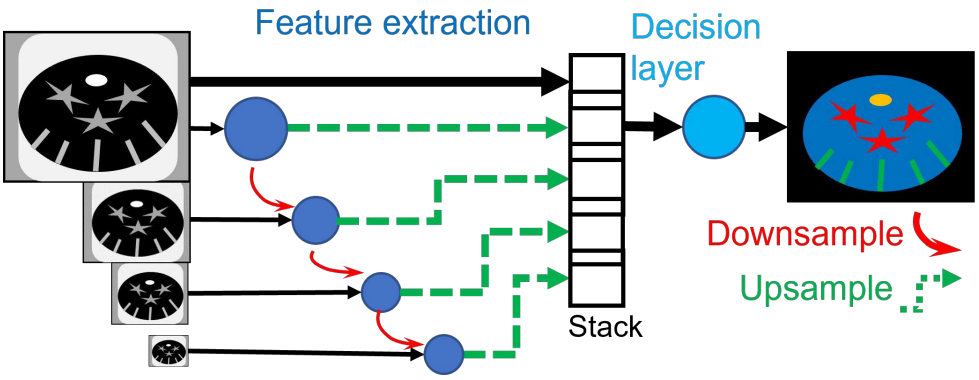


Fig. 6 Architecture of neural network model and forward method.

	Size	Stride	Layer	Activation
1	3x3	1	Padded conv	Leaky ReLU
1	3x3	2	Padded conv	Leaky ReLU
2	1x1	1	Conv	2-sided ReLU

Table 4 Parameters of the convolutional layers. Layers labeled (1) belong to the Feature Extraction Blocks, and layers labeled (2) belong to the Decision layer.

The specific architecture chosen, as seen in figure 6, is a modification on a U-net that down samples the original image as input at each block. This is inspired by the feature pyramid architecture which establishes the benefits of multi-resolution inputs. [15, 16] The other significant modification is the replacement of the upsampling convolutions of the U-net with a 1x1 transformer layer. This layer is fed directly by the resized output of each block. These changes are motivated by a prioritization towards speed and resource efficiency [17–19]. Convolutional parameters are also detailed in table 4.

The **forward method** of our model consists of sequential 3x3 convolutional blocks that halve the spatial dimensions before being passed to the next standard block. All block outputs are up-sampled to the original input size and concatenated together

before being passed to a final block known as the decision layer that produces the final output with the correct number of output channels.

The **feature extraction blocks** in our model consists of a series of convolutional filters. The Input of each block is a down-sampled copy of the original image concatenated to the output of the previous block. The output of each standard block is one-half the size of its input.

The **decision layer** is a single 1x1 convolutional layer that takes in the combined output channels of the feature extraction layers and outputs the correct number of prediction channels for each of the output label classes. The output of each layer is then clipped to (0,1) for evaluation and a two-sided leaky RELU on training. A soft dice loss coefficient was used as the loss function for training.

2.8 Data Augmentation

Data augmentation on training is key for model robustness and reducing overfitting. The input images were disturbed before being given to the network during training. This is accomplished using the following steps shown in table 5. Examples of augmented images can be seen in figure 7.

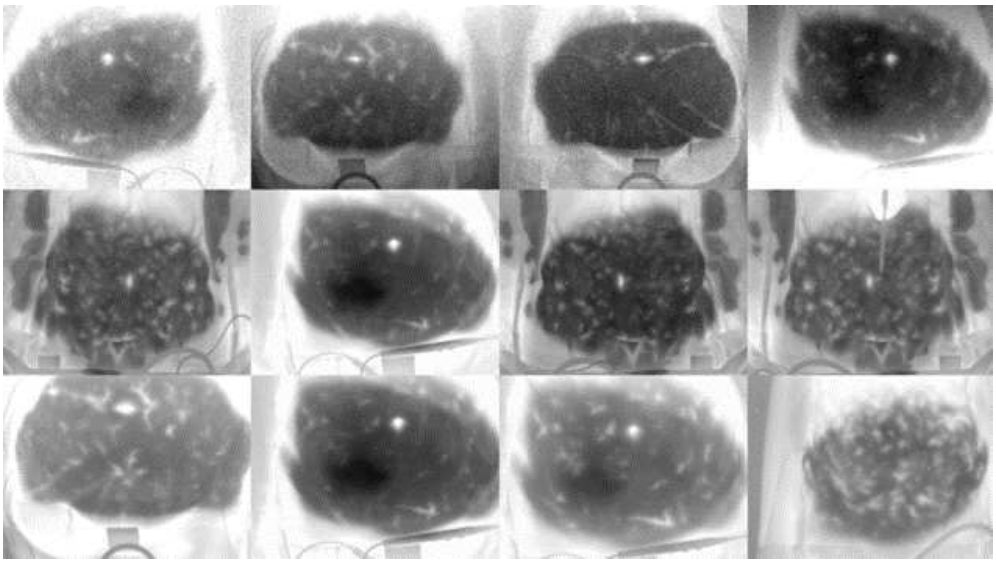


Fig. 7 Example of output of image augmentation for neural network training

Method	Value
Resizing	0.5-1
Cropping	200 x 200 pixels
Flipping	Horizontally
Rotating	-25 °- 25 °
Warping	Perspective
Distorting	Gaussian blur
Distorting	Shot noise

Table 5 Different methods of image augmentation used

3 Results

3.1 Segmentation Accuracy

In order to assess how the segmentation accuracy changes over the course of reheating, segmentation is applied to every time point of the dataset and compared with the results obtained from using the endpoint. Accuracy is measured using the dice score. As shown in figure 8, segmentation of the umbilicus remains consistent over time. Perforator accuracy crosses a dice of 0.8 after 2 minutes and 0.9 after 4 minutes.

3.2 Region Quantification

Using the corrected labeled image, the median temperature of each class is measured. As shown in table 9, the average intensity of the Umbilicus starts at 30°C and raises by 2°C. The abdomen starts at 7°C and heats to 20°C over five minutes. The cooling artifacts start at around 13°C and heats to 20°C over five minutes. The temperature of the cooling artifacts is slowly converging to the temperature of the abdomen. The perforators start at around 10°C and heats to 28°C within the five minutes. The perforators cross past the temperature of the artifacts around 1 minute into rewarming.

4 Discussion

The goal of this study was to detail a method with which DIEP flap thermographic images can be automatically segmented and quantified. A specific requirement is that this network should be fast and computationally inexpensive enough to occur in a local system to be used in real-time. The purpose of this is so that it can be integrated into an operating room in the future as well as during the post-operative period on the ward. Using traditional segmentation techniques, we have shown the ability to automatically segment images in internally controlled conditions. In order to create a more robust system, the labeled images were curated and augmented before being fed into a convolutional neural network. The use of this system additionally allows for detections earlier into the rewarming transition. In addition to segmentation, it is possible to quantify the intensity, shape and growth of the perforator regions to provide objective metrics for selection for surgery. This will prove an invaluable tool for introducing dynamic infrared thermography to the surgical community.

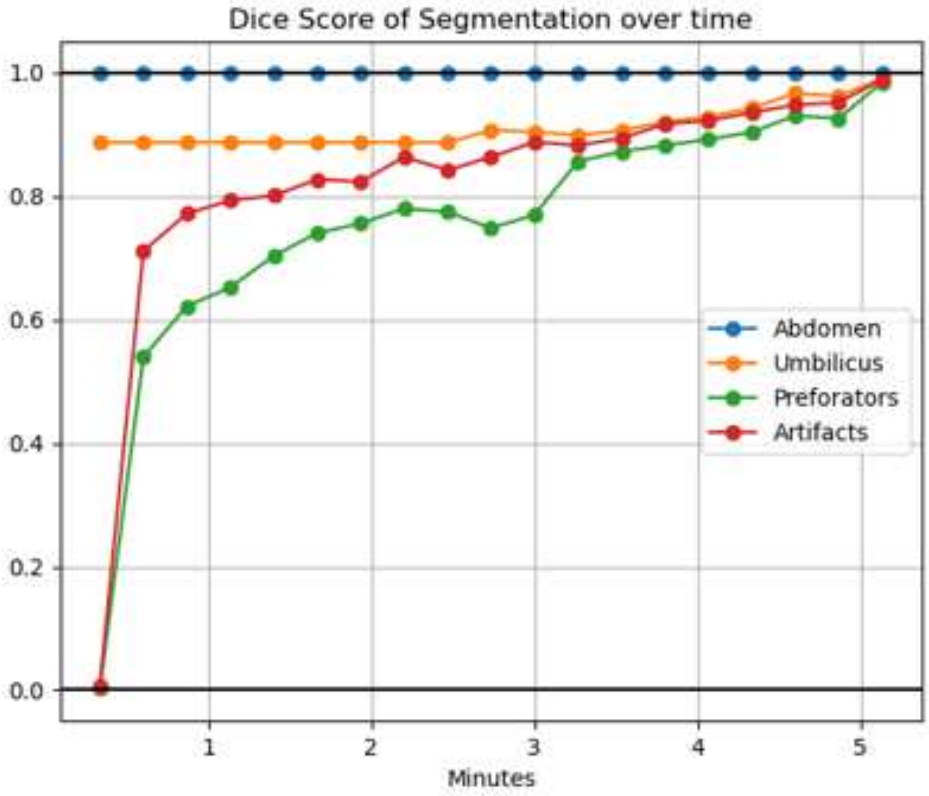


Fig. 8 Segmentation accuracy in dice loss of Neural network over time.

4.1 Computational Efficiency

In order to create a tool that might be used in a local system in real-time, steps were taken to create a solution that does not depend on a server or specialized hardware. Raw images taken from the camera were compressed to the effective frame rates (1Hz) and datatype (Uint8) to reach necessary conclusions while reducing over 90 percent of data size. Based on the results, this can be even further reduced to start and end timepoint images. Specific neural network architecture that is lightweight and computationally efficient is used to create a solution. The final evaluation speed of a 480 x 640 pixel image using a CPU is greater than 5 frames per second.

4.2 Future Work

Aspects of the study are not covered in this manuscript due to limitations on time, focus and scope. Future work includes the integration of the current analysis, which occurs after the fact, into a combined imaging system that can be used live during

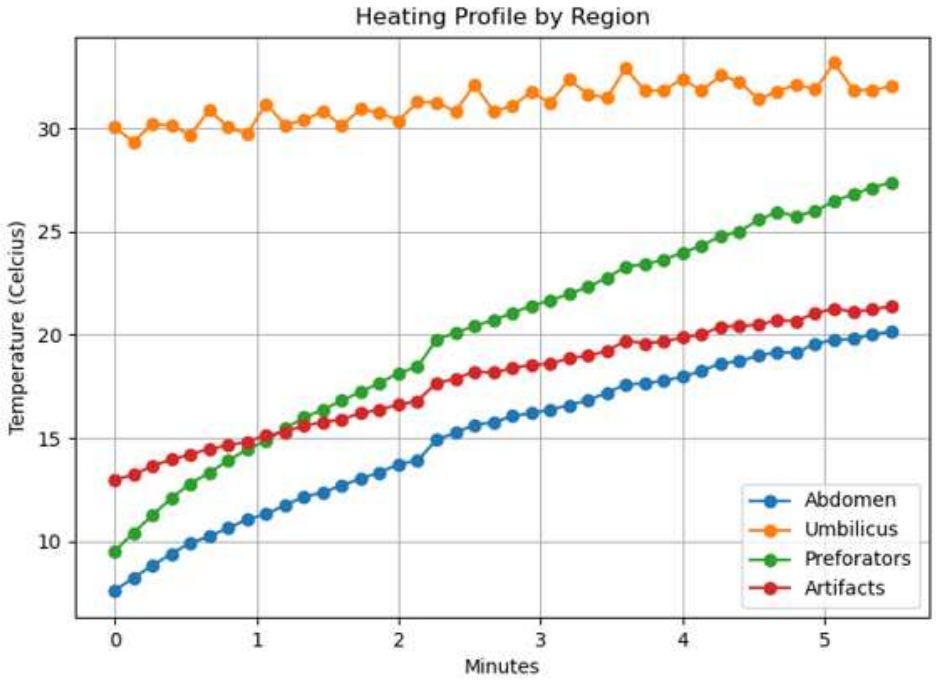


Fig. 9 Average temperature of each region in Celcius

the examination. Such a system might include a physical design that would standardize camera positioning, instead of the current tripod implementation so that imaging might be further standardized for other users. In the current study, all measurements used were taken during preoperative examination but thermographic measurements are also taken during the surgery (Perioperative) and after surgery (post-operative) care. Perioperative examination occurs after the skin to be translated is dissected except for the blood vessels feeding it. Perforator candidates are conducted by clamping each of the vessels and qualitatively examining the blood flow into tissue. This examination process requires at least 30 minutes during surgery and is currently a highly subjective process, therefore this examination procedure is a strong candidate for further investigation.

Acknowledgments. The authors thank the UZA medical and technical staff for their support on the preliminary measurements.

Declarations

Funding

This study was kindly supported by the Soroptimisten Anthos, Antwerp, Belgium. Research Foundation-Flanders under grant Doctoral (PhD) grant strategic basic research (SB 1SC0819N).
This research was funded by the Fund for Scientific Research (FWO) Flanders "Optimized skin tissue identification by combined thermal and hyperspectral imaging methodology." (FWO G0A9720N) This research was funded by the Fund for Scientific Research (FWO) Flanders (FWO G044420N).

Conflict of interest

The authors declare no conflict of interest

Ethics approval

The study was approved by the local ethics committee (B300201941125) and was carried out according to the Declaration of Helsinki (1983) Informed Consent Statement: "Informed consent was obtained from all subjects involved in the study."

Consent to participate

Informed consent was obtained from all individual participants included in the study.

Consent for publication

Patients signed informed consent regarding publishing their data and photographs.

Availability of data and materials

The dataset is available on request.

Code availability

Git	github.com/EdgarCardenasDeLaHoz/PerforatorDetection
License	MIT
Paid Dependency	None
Trained Model	Included
Datasets	On Request

Table 6 Software availability

Authors' contributions

Conceptualization: Edgar Cardenas De La Hoz, Filip Thiessen, Jan Verstockt;
Author: Edgar Cardenas De La Hoz and Jan Verstockt
Software: Edgar Cardenas De La Hoz;

Data curation: Jan Verstockt, Simon Verspeek and Filip Thiessen;
Supervision: Steve Vanlanduit and Gunther Steenackers;
Funding acquisition: Steve Vanlanduit and Gunther Steenackers;

References

[1] Sung, H., Ferlay, J., Siegel, R.L., Laversanne, M., Soerjomataram, I., Jemal, A., Bray, F.: Global Cancer Statistics 2020: GLOBOCAN Estimates of Incidence and Mortality Worldwide for 36 Cancers in 185 Countries. CA: A Cancer Journal for Clinicians **71**(3), 209–249 (2021) https://doi.org/10.3322/caac.21660 . _eprint: https://onlinelibrary.wiley.com/doi/pdf/10.3322/caac.21660. Accessed 2021-11-04

[2] Thiessen, F.E.F., Tondu, T., Cloostermans, B., Dirkx, Y.A.L., Auman, D., Cox, S., Verhoeven, V., Hubens, G., Steenackers, G., Tjalma, W.A.A.: Dynamic InfraRed Thermography (DIRT) in DIEP-flap breast reconstruction: A review of the literature. European Journal of Obstetrics & Gynecology and Reproductive Biology **242**, 47–55 (2019) https://doi.org/10.1016/j.ejogrb.2019.08.008 . Accessed 2022-10-14

[3] Kashyap, D., Pal, D., Sharma, R., Garg, V.K., Goel, N., Koundal, D., Zaguia, A., Koundal, S., Belay, A.: Global Increase in Breast Cancer Incidence: Risk Factors and Preventive Measures. BioMed Research International **2022**, 9605439 (2022) https://doi.org/10.1155/2022/9605439 . Publisher: Hindawi. Accessed 2023-05-24

[4] WHO: International Agency Research for Cancer, "Cancer WHOiafro. Estimated age-standardized incidence rates (World) in 2020, breast, woman, all ages (2020). http://gco.iarc.fr/today/home Accessed 2023-05-24

[5] Macadam, S.A., Bovill, E.S., Buchel, E.W., Lennox, P.A.: Evidence-Based Medicine: Autologous Breast Reconstruction. Plastic and Reconstructive Surgery **139**(1), 204–229 (2017) https://doi.org/10.1097/PRS.0000000000002855 . Accessed 2023-05-03

[6] Serletti, J.M., Fosnot, J., Nelson, J.A., Disa, J.J., Bucky, L.P.: Breast Reconstruction after Breast Cancer. Plastic and Reconstructive Surgery **127**(6), 124 (2011) https://doi.org/10.1097/PRS.0b013e318213a2e6 . Accessed 2023-05-03

[7] Unger, M., Markfort, M., Halama, D., Chalopin, C.: Automatic detection of perforator vessels using infrared thermography in reconstructive surgery. International Journal of Computer Assisted Radiology and Surgery **14**(3), 501–507 (2019) https://doi.org/10.1007/s11548-018-1892-6 . Accessed 2023-05-03

[8] Verstockt, J., Verspeek, S., Thiessen, F., Tjalma, W.A., Brochez, L., Steenackers, G.: Skin Cancer Detection Using Infrared Thermography: Measurement Setup, Procedure and Equipment. Sensors **22**(9), 3327 (2022) https://doi.org/10.3390/

s22093327 . Number: 9 Publisher: Multidisciplinary Digital Publishing Institute. Accessed 2022-05-11

[9] Thiessen, F.E.F., Vermeersch, N., Tondu, T., Van Thielen, J., Vrints, I., Berzenji, L., Verhoeven, V., Hubens, G., Verstockt, J., Steenackers, G., Tjalma, W.A.A.: Dynamic Infrared Thermography (DIRT) in DIEP flap breast reconstruction: A clinical study with a standardized measurement setup. European Journal of Obstetrics & Gynecology and Reproductive Biology **252**, 166–173 (2020) https://doi.org/10.1016/j.ejogrb.2020.05.038 . Accessed 2021-09-07

[10] Weum, S., Mercer, J.B., Weerd, L.: Evaluation of dynamic infrared thermography as an alternative to CT angiography for perforator mapping in breast reconstruction: a clinical study. BMC Medical Imaging **16**(1), 43 (2016) https://doi.org/10.1186/s12880-016-0144-x . Accessed 2021-06-07

[11] Mavioso, C., Araújo, R.J., Oliveira, H.P., Anacleto, J.C., Vasconcelos, M.A., Pinto, D., Gouveia, P.F., Alves, C., Cardoso, F., Cardoso, J.S., Cardoso, M.J.: Automatic detection of perforators for microsurgical reconstruction. The Breast **50**, 19–24 (2020) https://doi.org/10.1016/j.breast.2020.01.001 . Accessed 2023-05-03

[12] Kakileti, S.T., Venkataramani, K.: Automated blood vessel extraction in two-dimensional breast thermography. In: 2016 IEEE International Conference on Image Processing (ICIP), pp. 380–384 (2016). https://doi.org/10.1109/ICIP.2016.7532383 . ISSN: 2381-8549

[13] Thiessen, F.E.F., Tondu, T., Vermeersch, N., Cloostermans, B., Lundahl, R., Ribbens, B., Berzenji, L., Verhoeven, V., Hubens, G., Steenackers, G., Tjalma, W.A.A.: Dynamic infrared thermography (DIRT) in Deep Inferior Epigastric Perforator (DIEP) flap breast reconstruction: standardization of the measurement set-up. Gland Surgery **8**(6), 799–805 (2019) https://doi.org/10.21037/gs.2019.12.09 . Accessed 2023-05-03

[14] Guizar-Sicairos, M., Thurman, S.T., Fienup, J.R.: Efficient subpixel image registration algorithms. Optics Letters **33**(2), 156–158 (2008) https://doi.org/10.1364/OL.33.000156 . Publisher: Optica Publishing Group. Accessed 2023-05-03

[15] Ronneberger, O., Fischer, P., Brox, T.: U-Net: Convolutional Networks for Biomedical Image Segmentation. In: Navab, N., Hornegger, J., Wells, W.M., Frangi, A.F. (eds.) Medical Image Computing and Computer-Assisted Intervention – MICCAI 2015. Lecture Notes in Computer Science, pp. 234–241. Springer, Cham (2015)

[16] Lin, T.-Y., Dollár, P., Girshick, R., He, K., Hariharan, B., Belongie, S.: Feature Pyramid Networks for Object Detection. arXiv. arXiv:1612.03144 [cs] (2017). https://doi.org/10.48550/arXiv.1612.03144 . http://arxiv.org/abs/1612.03144 Accessed 2023-05-03

[17] He, K., Zhang, X., Ren, S., Sun, J.: Deep Residual Learning for Image Recognition. In: 2016 IEEE Conference on Computer Vision and Pattern Recognition (CVPR), pp. 770–778 (2016). https://doi.org/10.1109/CVPR.2016.90 . ISSN: 1063-6919

[18] Maas, A.L., Hannun, A.Y., Ng, A.Y.: Rectifier Nonlinearities Improve Neural Network Acoustic Models. 30th International Conference on Machine Learning (2013)

[19] Drozdzal, M., Vorontsov, E., Chartrand, G., Kadoury, S., Pal, C.: The Importance of Skip Connections in Biomedical Image Segmentation. In: Carneiro, G., Mateus, D., Peter, L., Bradley, A., Tavares, J.M.R.S., Belagiannis, V., Papa, J.P., Nascimento, J.C., Loog, M., Lu, Z., Cardoso, J.S., Cornebise, J. (eds.) Deep Learning and Data Labeling for Medical Applications. Lecture Notes in Computer Science, pp. 179–187. Springer, Cham (2016)